JOURNAL OF THERMOPHYSICS AND HEAT TRANSFER
Vol. 11, No. 4, October–December 1997

Heat Transfer and Flowfields in Short Microchannels Using Direct Simulation Monte Carlo

C. Mavriplis,* J. C. Ahn,† and R. Goulard‡
George Washington University, Washington, D.C. 20052

This paper explores the applicability of the Direct Simulation Monte Carlo (DSMC) method to the fluid and thermal analysis of microelectromechanical systems (MEMS). Flows in two-dimensional microchannels are investigated because they represent basic geometrical components of MEMS. Supersonic, subsonic, and pressure-driven, low-speed flows are simulated by DSMC in microchannels of varying aspect ratios for a range of continuum to transitional regime rarefied flows. Both hot and ambient wall temperature cases are presented. The results are strongly dependent on Knudsen number and channel aspect ratio. They are in qualitative agreement with other computational and experimental results for longer microchannels. Near the continuum limit, they show the same trends as classical theories, such as Fanno/Rayleigh flow and boundary-layer interaction with shocks. This investigation establishes DSMC as an efficient method for the analysis of MEMS: all simulations are carried out on a personal computer.

Nomenclature

h = channel height
L = channel length
P = pressure
T = temperature
U = streamwise velocity
x = length coordinate along channel wall
λ = mean free path

Subscripts
i = inlet
o = outlet
w = wall
∞ = freestream

I. Introduction

THE field of microelectromechanical systems (MEMS) has rapidly developed in the last several years.[1–3] From biomedical applications[4] to flow control devices,[5] the potential of MEMS has attracted the attention of many scientists and engineers. The advances in fabrication techniques have enabled the production of sophisticated microdevices. As an example, Guckel et al.[6] used a technique based on lithography and electroplating to fabricate a current excited planar rotational magnetic micromotor. Lammerink et al.[4] used surface micromachining to fabricate an integrated microliquid dosing system for drug dispensing, which consists of a micropump and a microflow liquid sensor. Tonucci et al.[7] and Pearson and Tonucci[8] fabricated arrays of micropipes with diameters as low as 17 nanometers that can be used as optical screens.

While fabrication techniques have developed at a fast pace, the understanding of the flow and heat transfer characteristics of MEMS has not. The microscales involved in these devices introduce operating regimes with which we are unfamiliar. Hence, much analysis is needed in this area. It is expected that further reduced scales in MEMS will require more refined analytical approaches. The aim of this paper is to establish the feasibility of applying efficient direct simulation Monte Carlo (DSMC) methods, traditionally used in high-altitude rarefied flows, to the microflows in and around microdevices.

Broadly speaking, the size h of current microdevices is in the range from a tenth of a micron to several hundred microns [$\mathcal{O}(10^{-7})$–$\mathcal{O}(10^{-4})$ m]. Because the atmospheric λ at standard conditions (STP) is roughly of the order of 5×10^{-8} m (but can rise for lower pressures and higher temperatures), it follows that the Knudsen number $Kn \equiv \lambda/h$ of the flow in and around recent microdevices ranges from 0.001 to near 1. In general terms, the continuum regime lies in the range of Knudsen numbers less than 0.01, and the free molecular (rarefied) flow regime corresponds to Knudsen numbers larger than 10. The regime in between, $0.01 < Kn < 10$, is the transition (rarefied) flow regime typical of many flows in and around microdevices.

In the continuum flow limit, there is a sufficient number of molecules within the smallest significant flow volume to justify statistically macroscopic flow properties such as velocity, density, pressure, and temperature. Under such circumstances, the Navier–Stokes equations with no-slip boundary conditions can generally be used. In the near-continuum flow regime, known as slip flow regime, the slip boundary conditions are used. Beskok and Karniadakis[9] used a spectral element Navier–Stokes equations solver with modified slip boundary conditions for simulating microchannel flows. The Navier–Stokes equations corrected for slip flow are valid up to Knudsen numbers of the order of 0.1.

When the flow is more rarefied (Knudsen number larger than 0.2), the continuum flow model is no longer valid and must be replaced by a molecular model where the volume is filled with a large number of discrete molecules. The governing equations of the flow model must change from the Navier–Stokes equations to the Boltzmann equation, which involves the molecular velocities instead of the macroscopic quantities. To solve this integro-differential equation for the velocity distribution function using conventional finite element or finite difference methods is difficult, since the number of independent variables include both those of physical space and those of velocity space. An alternative method for evading these difficulties is the direct physical simulation method that takes advantage of the molecular structure of gases and can handle

---

Presented as Paper 96-0361 at the AIAA 34th Aerospace Sciences Meeting, Reno, NV, Jan. 15–19, 1996; received June 21, 1996; revision received May 6, 1997; accepted for publication May 6, 1997. Copyright © 1997 by the American Institute of Aeronautics and Astronautics, Inc. All rights reserved.

*Assistant Professor, Department of Civil, Mechanical, and Environmental Engineering. Member AIAA.

†Graduate Student, Department of Civil, Mechanical, and Environmental Engineering. Student Member AIAA.

‡Emeritus Professor, Department of Civil, Mechanical, and Environmental Engineering. Member AIAA.

wide ranges of Knudsen numbers. One of these molecular dynamics simulation methods is the DSMC method developed by Bird.[10] Although many other methods have been developed recently, such as lattice gas automata (LGA) and cellular automata (CA), the DSMC method is being widely used for high-altitude hypersonic flows. Continuous improvements in efficiency and accuracy have been accomplished by Bird and his colleagues over the last several decades.[11–15] Further, as MEMS devices approach the 0.1-μm scale, flow regimes in and around these new devices are more rarefied than the slip flow regime and, hence, a direct simulation method such as DSMC is needed. We have found Bird's method[10] to be very efficient and practical. This study is aimed at showing the applicability of the established DSMC methodology for high-altitude rarefied flows to the analysis of MEMS flows.

We choose to investigate flows in microchannels because they represent a basic geometrical component of many MEMS and because experimental results are available.[16–18] Other computational investigations of microchannel flows have also recently appeared concurrently with our investigations: slip flow simulations[9] and DSMC simulations.[19,20] We compare our results to these in Sec. III, later in this paper.

II. DSMC Method

The DSMC method is a computer simulation method for practical gas flows, in which a real gas is simulated by thousands or millions of simulated molecules. The positions, velocities, and initial states of these simulated molecules are stored and modified in time in the process of molecules moving, colliding among themselves, and interacting with boundaries in simulated physical space. The simulation time of the DSMC method is a real physical time and all DSMC calculations are treated as unsteady, even though the boundary conditions may be given in the steady state. The solution of the steady-state case is the asymptotic limit of the unsteady flow.

In the DSMC method, each simulated molecule represents a very large number of physical molecules. In this fashion, the number of molecular trajectories and molecular collisions that must be calculated is substantially reduced, while the physical velocities, molecular size, and internal energies are preserved in the simulation. Further, the DSMC method uncouples the analysis of the molecular motion from that of the molecular collisions, by using a time step smaller than the real physical collision time.

Bird's DSMC procedure is based on a scheme composed of the following steps: it cycles the movement of molecules, indexes molecules into cells, selects collision pairs, and calculates postcollision properties. The flowfield and surface quantities are sampled repeatedly, starting from the initial data. The basic flow chart of the conventional DSMC method is given in Ref. 10.

In Bird's DSMC method,[10] the physical space is divided into a certain number of cells, and each cell is also divided into subcells (distinct from conventional finite element or finite difference methods). The physical space network is used to facilitate the choice of molecules for collisions and for the sampling of the macroscopic flow properties such as pressure, temperature, etc. The time step is chosen so that a typical molecule moves about one-third of the cell dimension at each time step. Also, this time step is much less than the mean collision time, which is defined as the mean time between the successive collisions suffered by any particular molecule.

III. DSMC Simulation

Two-dimensional or axisymmetrical microchannels are typical components of conventional microelectromechanical systems. There are many examples of flows in MEMS components that may be modeled as two-dimensional microchannels, such as the flow in the gap between the rotor and stator in Guckel et al.'s micromotors.[6] Similarly, the flow through the arrays of nanoscale micropipes with an aspect ratio of 2.5 (Refs. 7 and 8) can be assumed to be micropipe flow.

The specific case of two-dimensional microchannel array flows is simulated in this study. Detailed flow property distributions (i.e., pressure, density, velocity, temperature, etc.) are obtained. First, the supersonic flow through a two-dimensional infinite array of microchannels is simulated. We start with supersonic continuum flow to validate our DSMC results. A range of Knudsen numbers and several channel lengths are investigated. Second, subsonic flow through the same microchannel array for the same Knudsen numbers and channel lengths, is simulated and heat transfer and flow properties are discussed. Finally, the pressure-driven flow through the same microchannel array is simulated and results are compared to those of other investigations.

The basic premise of microchannel modeling by the DSMC method is that molecular gas motion is the same if the Knudsen number is the same and the boundaries are geometrically similar. This means that the basic (intensive) flow properties are independent of the size of the channel model if the same Knudsen number conditions are maintained. Similarity is used to avoid roundoff errors since the real sizes involved in these microgeometries are quite small. Therefore, we study fairly large diameters [$\mathcal{O}(10^{-2})$ m], but at a lower initial pressure (or number density) than the actual pressure (or actual number density) to maintain the same Knudsen number as in the case of the real microchannel. The dimensional output of flow properties such as pressure, shear stress, and heat transfer are adjusted in postprocessing procedures.

In this study, the DSMC simulation models are all infinite arrays of microchannels with symmetry (specular) boundary conditions at both upper and lower surfaces of the computational domain. Each cell is divided into two subcells in each direction. The time step is also chosen so that a typical molecule moves about one-third of the cell dimension at each time step. The variable hard sphere (VHS) model[10] and nitrogen gas were used in all simulations.

A. Supersonic Microchannel Flow

The supersonic flow of nitrogen gas in a microchannel array is simulated for a freestream Mach number is 4.03 ($U_\infty = 1400$ m/s, = $T_\infty = 300$ K), and channel wall and freestream temperatures of 300 K. The channel wall is modeled as a diffusely reflecting surface. The results are presented for three Knudsen

Table 1 Basic input data of DSMC calculation for the supersonic channel flow[a]

	Case		
	1	2	3
Kn	0.004622	0.04622	0.1849
Channel depth/2 ($h/2$, μm)	52	0.52	0.13
Number of cells in channel	4940	2000	500
Number density, mol/m^3	7×10^{22}	7×10^{20}	1.75×10^{20}
Initial number of molecules in each cell	10	10	10
Number of subcells in each cell in each direction	2	2	2
Time step (Δt)	3×10^{-8}	1.25×10^{-6}	2.5×10^{-6}

[a] $M_\infty = 4.03$ and AR = 2.5.

numbers, corresponding to three channel sizes given in terms of channel depth h for a fixed aspect ratio $AR \equiv L/h = 2.5$. The basic DSMC input data for these three cases are shown in Table 1. These three cases span the near continuum (1) to the transitional regimes (2) and (3), with case 3 being the most rarefied. Case 1 is used for validation: in the continuum range the theory is demonstrated in a clear way.

The grids chosen for each case are shown in Fig. 1. Only the lower half of one channel is simulated and shown: the lower white rectangle is the solid part of length L and the gridded part represents, from left to right, the flow before, inside and after the solid structure. The upper boundary of the grid coincides with the horizontal plane of symmetry of the flow. Its ordinate is therefore half the channel depth: $h/2$. Basically, the choice of cell size depends on the Knudsen number and flow gradients. The mesh for case 1 has 50 × 70 square cells near the shock area, and 20 × 72 for the rest of it with varying cell size (1:4). Case 2 has 20 × 100 square cells, and case 3 has 10 × 50 square cells. The fine grid in case 1 (the near continuum case) is needed to capture the thin bow shock ahead and in the entrance region of the channel. These meshes represent our final mesh choices after careful validation of the results by refining the grid and varying the number of molecules per cell until independence from these parameters was achieved for each case.[21]

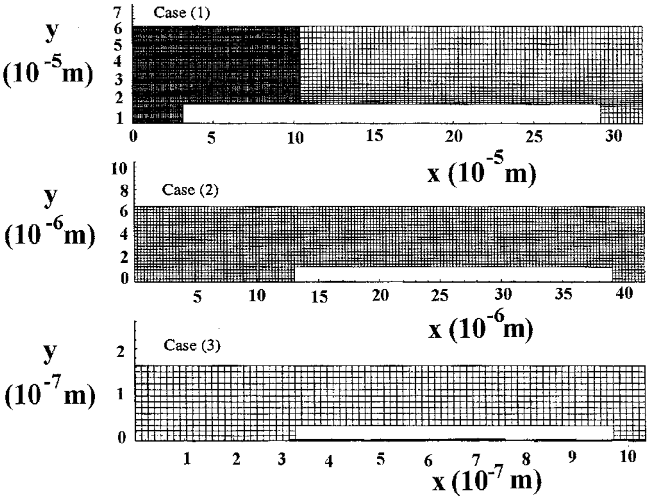

Fig. 1 Grids for supersonic microchannel flows.

Figure 2 shows DSMC results for the pressure distribution in the flow, and Fig. 3 illustrates the surface (wall) heat flux profiles for each of the three cases. As the Knudsen number becomes larger, the flows are more rarefied and the effect of intermolecular collisions is reduced; hence, molecule/surface interactions become relatively more important.

The shock thickness is of special interest. It is a function of the freestream Mach number, the viscosity temperature index, and the molecular mean free path.[22] Figure 2 displays the broadening of the shock as the Knudsen number (or the molecular λ) increases.

Case 1 exhibits a fairly strong bow shock in front of the channel inlet. Actually, there are two bow shocks entering the channel, because the boundary condition of the upper edge of the domain is one of symmetry. This is equivalent to having a reflected oblique shock on the plane of ordinate $h/2$ parallel to the lower channel surface. A full-channel model has been made and reveals the same results.[21] These two bow shocks merge at approximately 24 μm down the channel. A reflected oblique shock impinges on the lower channel wall at approximately 100 μm down the channel. Because of the presence of a boundary layer, the reflected oblique shock bends at its intersection with the boundary-layer edge and vanishes at the sonic line inside the boundary layer. These shock–boundary interaction effects propagate upstream in the subsonic boundary layer. As a result, the pressure in the boundary layer begins to rise before the point of shock impingement (100 μm down the channel). Because of the pressure rise in the boundary layer, the velocity there decreases; hence, the boundary layer thickens from the channel inlet to 100 μm down the channel. This matches the continuum results shown in Chaps. 16 and 28 of Ref. 23. As mentioned earlier, when the flow becomes more rarefied (cases 2 and 3), the bow shock becomes thicker. The bow shock has thickened to one-quarter of the channel depth in case 2. In case 3, the shock thickness is of the same

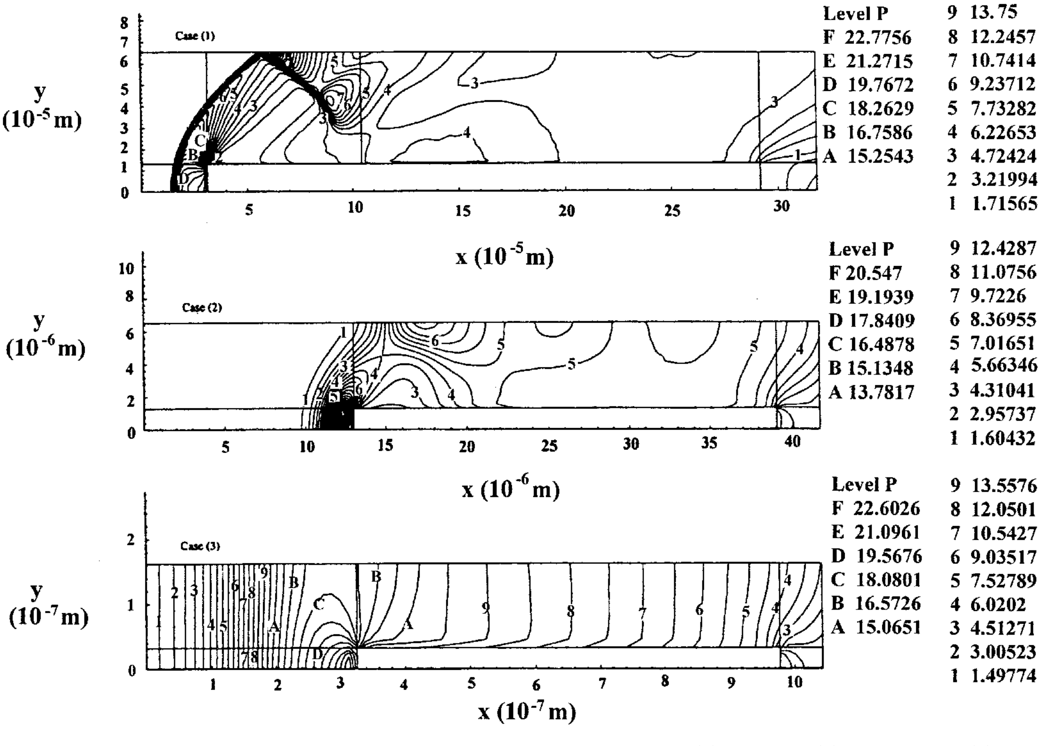

Fig. 2 Pressure contours of supersonic microchannels [AR = 2.5; Kn = 0.0004622 (1), 0.04622 (2), and 0.1849 (3); and M_∞ = 4.03].

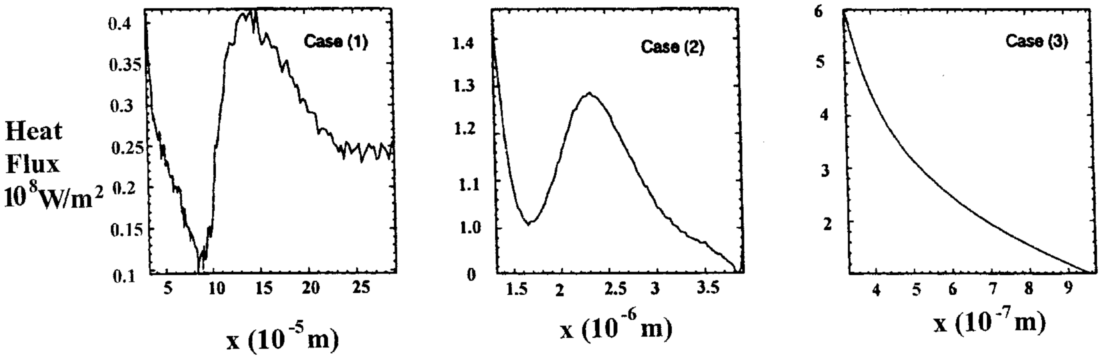

Fig. 3 Surface heat flux (W/m^2) of supersonic microchannels [AR = 2.5; Kn = 0.0004622 (1), 0.04622 (2), and 0.1849 (3); and M_∞ = 4.03].

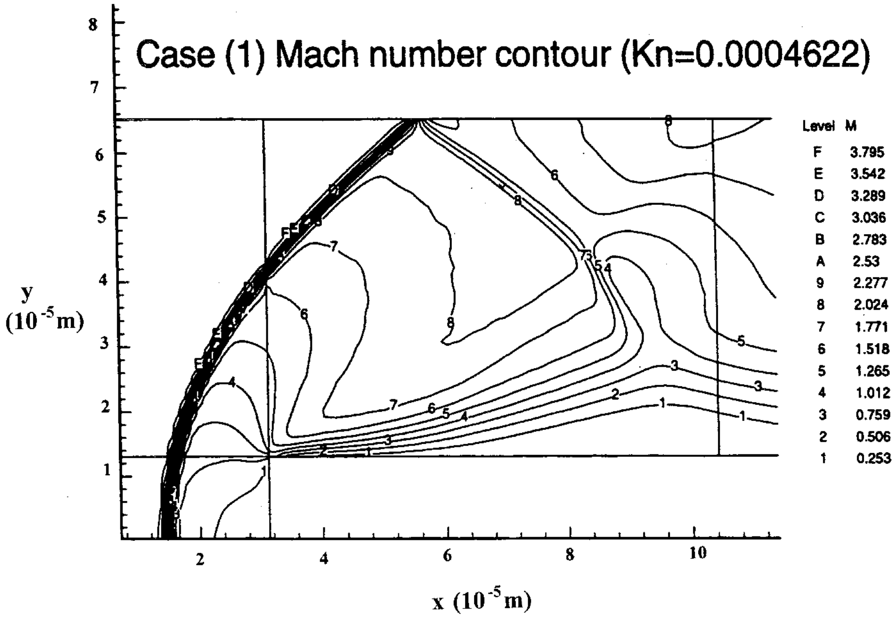

Fig. 4 Mach number contours of supersonic microchannels (AR = 2.5, Kn = 0.0004622, M_∞ = 4.03).

order as the channel height, and it has spread far upstream of the channel inlet. The resulting flow inside the channel is almost exclusively subsonic.

In case 2, the reflected shock is also diffuse; hence, there is a relatively small impingement on the lower wall. In Fig. 3, cases 1 and 2 reveal that the heat flux suddenly increases about halfway downstream because of the effect of the reflected shock. At these points, the density increases, thereby increasing the heat transfer. In case 3, the reflected shock has disappeared and the heat flux at the channel wall is simply monotonically decreasing as the flow is fully subsonic in the channel. Because of the large surface/volume ratios inherent to microdevices, a good understanding of surface effects (such as heat transfer as illustrated here) may become critical.

From the Mach number contours of case 1 near the plane of symmetry, the angle of the oblique shock is 42 deg and the deflection angle is 27 deg (Fig. 4). This case corresponds to an upstream Mach number M_∞ = 4.03. For these values of M_∞ and oblique shock angle, the deflection angle, from classical continuum theory[24] is 28 deg, very close to the DSMC result of 27 deg.

Similarly, the simulated downstream Mach number behind the shock is between 2.0–2.3 (levels 8 and 9 in Fig. 4), not far from the continuum theoretical Mach number of 2.0. Note also that oblique shock theory shows that a M = 2 flow cannot turn through a reflected straight shock by more than 23 deg. It is then expected that for the 28-deg turn required by the return horizontal flow at the plane of symmetry (Fig. 4), both oblique and reflected shocks will curve and merge into a shock normal to the plane of symmetry.[24] This well-known effect is visible in Fig. 4 (and much more so in Figs. 14 and 16 of Ref. 21).

To examine the effect of channel length in the transition flow regime (cases 2 and 3), longer supersonic flow microchannel models are simulated, with the same depth h, but a longer length L, and therefore, larger aspect ratios (AR = 5, 10, and 20). The boundary and initial conditions are the same as in the preceding cases (2 and 3). Figure 5 exhibits the pressure drop and heat flux along the channel surface of case 2 for AR = 5, 10, and 20.

The longer channel cases (AR = 5, 10, and 20) are somewhat different from the shorter channel cases (see Fig. 5). The inside channel flow is fully subsonic,[21] and the bow shock has become broadened and has moved far upstream of the channel inlet compared to the short channel cases shown in Fig. 2. This may be the effect of channel length: the boundary-layer thickness increases with increasing channel length. Hence, the ratio of the boundary-layer thickness to the channel height increases compared with that of the short channel. The total wall friction also increases with increasing channel length. Both (coupled) effects retard the flow entering the channel inlet, and reduce the stream velocity through the channel. Therefore, the velocity inside the channel is completely subsonic and the heat flux decreases monotonically. For the longer case 2 channels in Fig. 5, the heat flux trend at the channel wall is also different from that of the shorter case 2 channel in Fig. 3. The heat flux decreases monotonically instead of showing a sudden increase as in the short length channel case; this trend is almost iden-

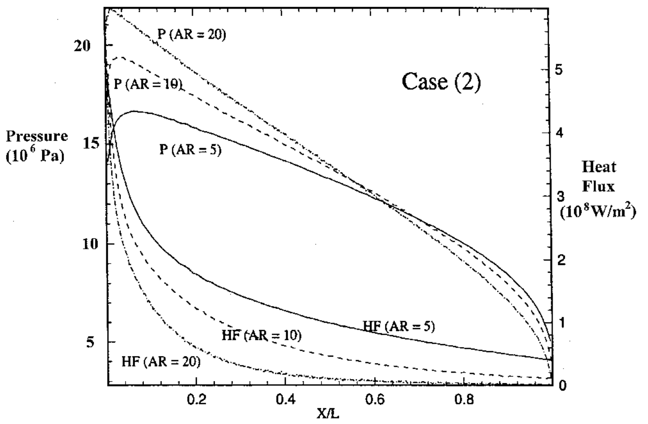

Fig. 5 Pressure (P) drop and heat flux (HF) for supersonic microchannels (AR = 5, 10, and 20; Kn = 0.04622; and M_∞ = 4.03).

tical to case 3 in Fig. 3. In Fig. 5 (AR = 5, 10, and 20), the inlet pressure at the channel surface increases as the channel length becomes longer. Consequently, the effect of channel length in supersonic flow has a similar trend to that of a more rarefied flow through the channel (the shock has moved forward of the channel entrance and the heat flux decreases monotonically). In other words, the increased wall shear, because of a longer wall, has the same effect as an increased molecular wall impingement in rarefied flows past walls of a given area.

A similar investigation was carried out in Ref. 20. The main differences between our work and that of Ref. 20 are that they use $M_\infty = 5$, $T_\infty = 298$ K, $Kn = 0.065$, 0.13, and 0.19 flows in microchannels of AR = 5, with 1 mm length of domain ahead of the channel modeled with prescribed freestream velocity at inflow and specular surfaces ahead of the channel walls (at the same height). They also use a new DSMC method based on a Lagrangian grid for the particle simulation, and the calculations are carried out on a massively parallel supercomputer (CM-5). While we cannot directly compare our results to those of Ref. 20 because of the physical differences in simulated cases, we do believe that we have obtained qualitatively similar results with considerably less effort on a personal computer.

B. Subsonic Microchannel Flow

The subsonic channel flow is also simulated in this study by modeling an infinite array of two-dimensional microchannels with the same boundary conditions as in previous supersonic channel cases: the aspect ratios are 2.5, 5, 10, and 20, and the Knudsen numbers are the same as those of supersonic cases 2 and 3. The basic DSMC input data for subsonic and aspect ratio 2.5 are the same as for the supersonic flows (see Table 1).

The freestream Mach number is 0.4 (U_∞ = 138.8 m/s, T_∞ = 300 K). The channel wall is modeled as a diffusely reflecting surface and has a fixed temperature T_w = 300 K. Figure 6 shows the pressure at the channel wall for case 2. Case 3 shows similar trends as case 2.

In the subsonic flow (M_∞ = 0.4), the Reynolds number is lower than that of previous supersonic flow cases. Hence, the boundary-layer thickness of subsonic channel flows is thicker than in the supersonic flow case; there is a relatively larger momentum loss for the incoming flow. Thus, for small channel inlet dimension, the effect of this retarding force is more severe, compared to the high-speed flow cases. From the pressure contours,[21] we can observe a rapid compression ahead of the channel inlet. Also, the streamwise velocity through the channel is less than the freestream velocity.[21] Both phenomena are a result of the retarding force. The ratio of compression thickness to the channel height of case 3 is larger than that of case 2, because the ratio of boundary-layer thickness to channel height is bigger than that of case 2. Hence, the streamwise velocity through the channel in case 2 is slightly larger than in case 3, which is more rarefied.

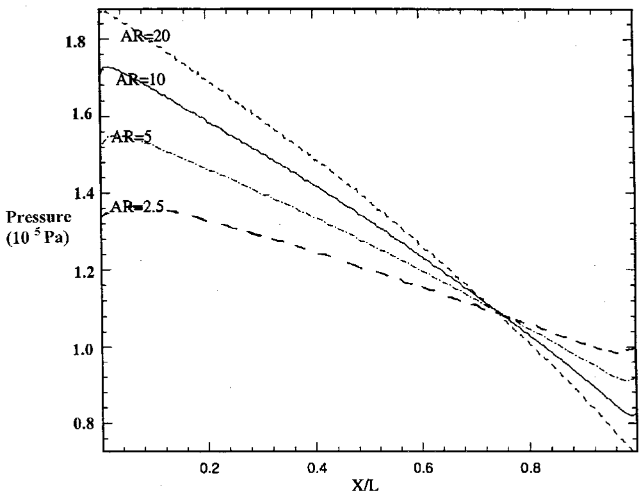

Fig. 6 Pressure drops through the subsonic microchannels of case 2 (AR = 2.5, 5, 10, and 20; Kn = 0.04622; and M_∞ = 0.4).

The heat flux along the channel wall decreases rapidly and maintains a weak (almost zero) heat flux for a large part of the channel. The weak heat flux zone begins at the same abscissa x (about 1 μm, for all of the aspect ratios tested in case 3). Therefore, it gets longer as the channel length increases. It is evident that the wall temperature is almost constant and does not vary much in the subsonic cases. Because the aspect ratios of real MEMS microchannels are very large (e.g., 3000 for Ho's model[17,18]), the adiabatic zone (constant temperature zone in this case) is spread practically throughout the channel length. Therefore, these results show that the initial isothermal flow assumption that is generally used in analytical approaches is valid.

Also, there is no evidence of a rapid pressure surge at the inlet and drop at the exit, which happen in continuum and slip flow regimes, since the relatively long λ compared to the channel dimension h (large Kn) precludes entrance and exit effects. As it was the case for the supersonic cases, Fig. 6 shows that the inlet pressure of the channel for case 2 increases as the channel becomes longer, because of the increased boundary-layer thickness and to the resultant retarding forces throughout the channel. The channel length effects in case 3 have a trend similar to those in case 2, while the inlet pressure is higher than in case 2, for each aspect ratio.[21] Hence, the ratio of inlet pressure to exit pressure increases with increasing channel length, for a given exit pressure.

Next, subsonic flow cases are simulated for different surface and freestream temperatures, to study the cooling behavior of the microchannel. The freestream temperature is 300 K and the surface temperature is 600 K. The pressure drop and heat flux at the hot channel surface are shown in Fig. 7 for case 2 (Kn = 0.04622). (The heat flux shown is from the stream to the wall. It is therefore negative in this hot wall case. Zero heat transfer corresponds to the top of Fig. 7.)

In Fig. 7, the results for aspect ratios of 5, 10, and 20 show that almost all heat transfer occurs at the inlet and near the exit of the channel where the temperature differences are largest. In the AR = 2.5 case, heat transfer occurs throughout the channel because of its relatively short length. Pressure at the channel inlet is also higher than in the isothermal (cold surface) case, because increasing stream temperature means increasing pressures at the molecular level.

Similarly, rises in both exit pressure and (negative) heat transfer are a result of upstream molecular diffusion in this subsonic case. Hence, for AR = 5, 10, and 20, minimal heat fluxes are predicted in the middle section of the channel: most of the cooling of the microchannel occurs at the inlet and near

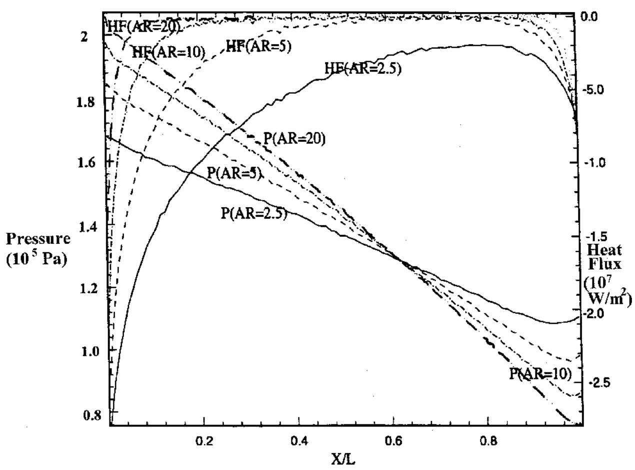

Fig. 7 Wall pressure drop and heat flux for hot surface subsonic microchannel flow (case 2, AR = 2.5, 5, 10, and 20; *Kn* = 0.04622; and M_∞ = 0.4).

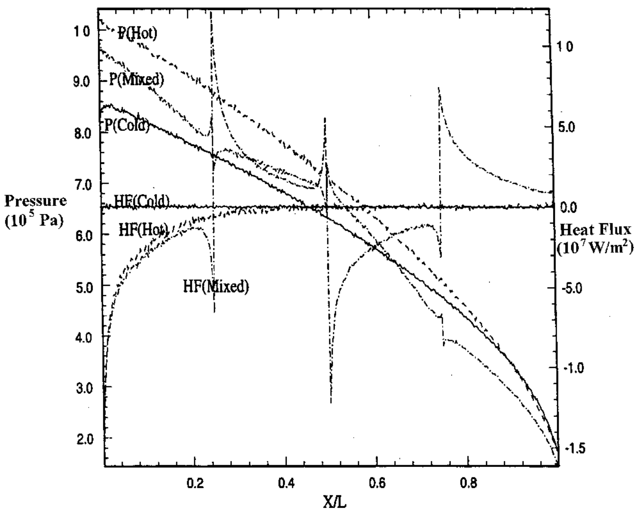

Fig. 8 Wall pressure drop and heat flux for cold, mixed, and hot surface pressure-driven microchannel flow.

the exit of the channel. Designers face this significant factor when designing efficient micro-heat-exchangers

C. Pressure-Driven Microchannel Flow

We consider an infinite array of two-dimensional pressure-driven channels, with 0.5 μm depth, fixed aspect ratio AR = 10, and an inlet/exit pressure ratio of 8 (i.e., from 8 × 10^5 Pa to atmospheric: 10^5 Pa). This case is similar to the experimental model (JH6) of Pfahler et al.[16]

The basic input data for DSMC calculation is as follows: The boundary conditions are specified flow for constant pressure (8 atm at upstream boundary, and a little less than 1 atm at downstream boundary to obtain 1 atm at the exit of the channel) via molecules generated by the appropriate Maxwellian distribution for that flow.[25] The pressure ratio (P_i/P_o) is 8, the channel depth is 0.5 μm, the number of cells in the channel is 8000, the number density is 2.7 × 10^{21} molecules/m,[3] the initial number of molecules in each cell is 10, the number of subcells in each cell in each physical (x- y) direction is 2 (for a total of 4 per cell), and the time step is 1.25 × 10^{-6} s. Nitrogen gas is used and the channel wall is assumed to be a diffusely reflecting surface. The entry gas temperature is 300 K.

Three types of pressure-driven channel flows are simulated in this study: cold (300 K), hot (600 K), and mixed surface temperatures (in which the wall is divided into four sections and the temperature of each section is 600, 300, 600, 300 K, respectively). Fig. 8 shows the pressure drops and heat flux contours of the pressure-driven channel (cold, hot, and mixed surface temperatures).

In the cold surface case (Fig. 8), we see a rapid pressure drop throughout the channel because of viscous dissipation. The sudden pressure drop from 1.6 to 1.0 atm occurs within 10^{-2} μm of the channel exit; this trend seems to be similar to Beskok and Karniadakis's result,[9] though we are not using the same conditions: the pressure ratio is 8.0 for this study and 2.02 for Beskok and Karniadakis's case.[9] The AR is 10 for this study and 20 for Beskok and Karniadakis's case.[9] In addition, the pressure is dropping linearly until approximately half of the channel length, whereas the temperature[21] maintains an almost constant value (300 K); i.e., the initial temperature. And since the wall temperature is assumed to be also 300 K, the heat flux through the channel surface is almost zero. These results correspond to those of Beskok and Karniadakis.[9] They also seem to fit the trends predicted by the Fanno theory: beyond 40% of the channel length from the inlet, the Mach number (and the streamwise velocity) also increases rapidly and the pressure drop accelerates because of rarefaction effects. So we must consider compressibility effects in this region. However, the Mach number is nowhere near unity (Fig. 45 from Ref. 21); thus, no choking was observed. These trends also agree well with the results of Arkilic and Breuer.[26]

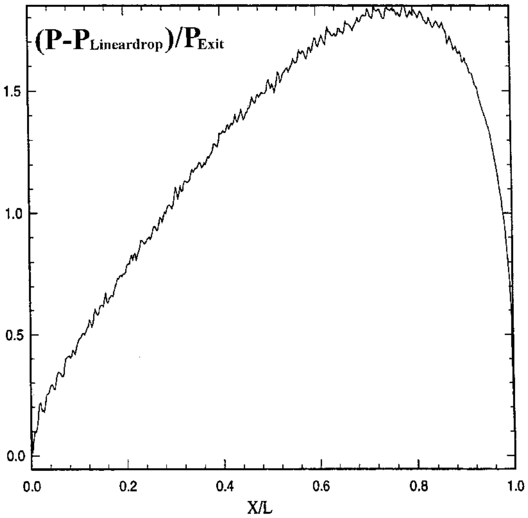

Fig. 9 Deviation of calculated pressure from linear pressure drop in pressure-driven microchannel flow.

Deviations from a linear pressure drop for nitrogen flow are shown in Fig. 9. Compared to Beskok et al.'s results,[27,28] the present study shows the maximum deviation located closer to the exit of the channel. Differences between these results may be caused by the different lengths of the channel, to the different pressure ratios as previously mentioned, or to the effect of a relatively short modeled section after the outlet of the channel.

Arkilic and Breuer[26] derived an analytical expression for the pressure drop along microchannel walls; a comparison with this study's results is shown in Fig. 10. The differences between the results may be because of the small aspect ratio of the channel. Because Arkilic and Breuer[26] derived analytical equations as an expansion in aspect ratio, the relatively short channel length (AR = 10) explains the deviation from this study's model. However, the basic trends are in fairly good agreement. The pressure distribution along the channel surface drops nonlinearly. References 17 and 18 experimental results have also shown nonlinear pressure drops; however, it is inappropriate to compare results since the aspect ratios here are much smaller than in Refs. 17 and 18 experiments (around 3000).

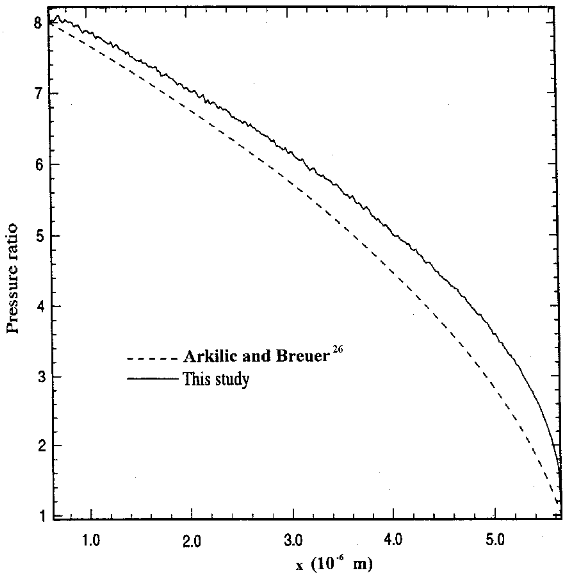

Fig. 10 Comparison of calculated pressure drop in pressure-driven microchannel flow with that of Arkilic and Breuer.[26]

Next, a hot surface pressure-driven microchannel flow is simulated in this study. The surface temperature is maintained at 600 K and the freestream temperature is 300 K. Figure 8 shows that for the hot surface case, the surface pressure at the channel inlet is higher (10 atm) than in the cold surface case (8 atm). This is a result of the stream temperature increasing above 300 K as it approaches the channel entrance. Because both the pressure and temperature reflect the increase of molecular velocity imparted by the hot wall, an increase in pressure is also observed in the channel entrance area (~10 atm). Therefore, the pressure drop (10 to 1) is also larger than in the cold surface case (8 to 1). Inside the channel, the temperature increases rapidly, to be equal to that of the wall (Fig. 49 from Ref. 21). Hence, the heat transfer is maximum at the channel inlet where the temperature difference is the largest while the rest of the channel maintains a temperature close to that of the wall: little heat transfer is taking place there. These observations are analogous to those made in Sec. III.B. The near-adiabatic middle section grows larger as the aspect ratio increases.

Finally, the case of variable wall temperatures (locally heated microchannel surface) for a pressure-driven microchannel is simulated. The microchannel surface is divided into four sections. Temperatures of the first and the third section are 600 K, and those of the second and fourth section are 300 K, which is the same temperature as that of the freestream. Total pressure drop at the channel surface (9.4 to 1) is less than in the case of a uniform high-surface temperature case ($T_w = 600$ K), where it is 10 to 1. It is higher, however, than in the cold surface case (8 to 1). Figure 8 shows also that the pressure drops rapidly in the hot surface sections and relatively less in the cold surface sections. Also, from the velocity profiles and the streamwise velocity contours,[21] the variation of streamwise velocity in the cold surface region is less than that in the hot surface region. From the Mach number contours,[21] the Mach number also increases more rapidly in the hot surface sections. Heat transfer is obviously maximum at the boundary of the first and the second sections, where the temperature difference is the biggest (600–300 K) (Fig. 8).

Figure 11 shows the temperature contours of the pressure-driven channel flows for the cold, hot, and mixed surface temperature cases. As can be observed, the temperature changes very little throughout the channel in the cold surface case, whereas almost all variations of temperature occur near the channel inlet in the hot surface case.

The mixed (hot and cold) surface case shows that most changes in temperature occur immediately downstream of the juncture between hot and cold surfaces, as expected. Further downstream in each zone, the stream temperature is adjusted to that of the wall. Hence, most heat transfer occurs at the zones near the boundaries, and fast cooling in the initial section of the cold region of the channel leaves no energy to heat the rest of the cold surface. The temperature contours in Fig. 11 illustrate that there are negligible heat transfer and small temperature changes in the cold surface case, while the heat transfer is maximum near the channel inlet or near the discontinuous temperature boundary zones of the mixed surface case. Although this last case is not meant to approximate a realistic heat exchanger, it sheds some light on the convective cooling of a plate with a variety of surface heat sources as, for example, in the electronic chip component operation in MEMS devices.

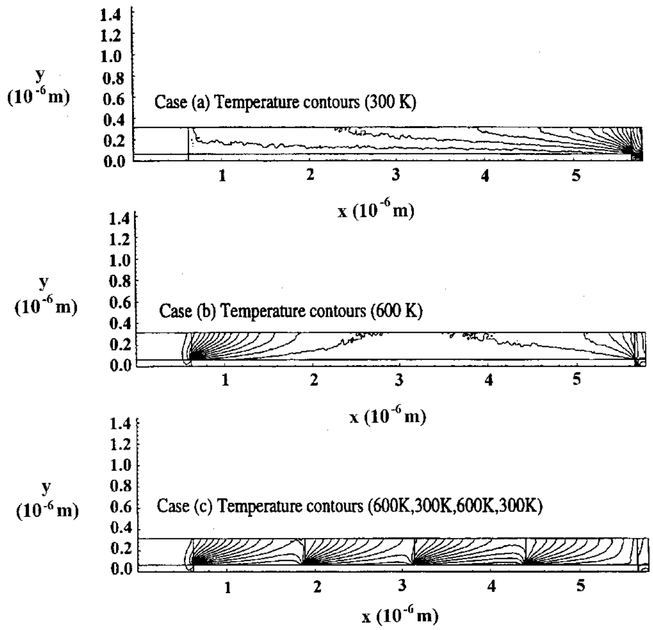

Fig. 11 Temperature contours of pressure driven microchannel with (a) cold, (b) hot, and (c) mixed surface temperatures.

IV. Conclusions

Several cases of microchannel flow have been simulated by DSMC. The near continuum supersonic flow case shows good agreement with continuum oblique shock theory. The shock–boundary interaction effect displayed by the DSMC solution also agrees well with theoretical and experimental results. Heat fluxes at the channel surface depend on the Knudsen number and channel length. As the Knudsen number increases, the shock broadens, the heat flux decreases monotonically along the channel wall, and the flow becomes fully subsonic in the channel. The inlet pressure of the channel also increases as the Knudsen number increases, because of the broadening of the shock. Hence, channel inlet dimension will play a significant role in high-speed flows in and around MEMS. The channel length also affects the microchannel flow. As it increases, the flow inside the channel becomes subsonic and the heat flux through the channel wall decrease monotonically. The inlet pressure also increases as the channel length increases because of increasing retarding force.

In the subsonic flow cases, the Reynolds number decreases; hence, the ratio of the boundary-layer thickness to the channel depth increases. Therefore, there is compression of the flow far upstream of the channel inlet. Also, the DSMC Mach number and temperature contours show good agreement with the trends of the Fanno/Rayleigh theory.

In the pressure-driven channel flow, the pressure distribution at the channel wall shows a linear decrease in the first 40% of the channel and a nonlinear decrease for the rest of the channel. Also, the temperature contours show that the temperature rapidly reaches the wall temperature value; hence, no heat transfer is expected farther downstream. Most experiments use very long channels compared to the diameter of the inlet (high aspect ratios, such as 3000): these experimental data cannot be directly compared with these DSMC results. Because of limited computer CPU speed and available memory size of personal computers, simulation of high aspect ratio channel flows was not possible in this study. However, the main trends of heat flux and macroscopic flow properties are in good agreement with experimental and theoretical results.

In the work described, it has been shown that the DSMC method can provide very detailed macroscopic heat and flow property distributions for rarefied flow in and around MEMS. This was done at relatively low cost, mainly because of the suitability of the DSMC method to personal computers and workstations. Complex geometries can be handled by using an unstructured mesh-generating scheme or by dividing the computational domain into many zones. It is hoped that in the not too distant future, as the performance of personal computers or workstations increases, the DSMC method will play an important role in the performance prediction and the design of microscopic structures with heat exchange requirements.

Acknowledgments

We thank G. A. Bird of the University of Sydney, who provided the DSMC G2 code and valuable advice. J. N. Moss and R. G. Wilmoth of NASA Langley Research Center, through many thoughtful discussions, have contributed greatly to our progress. We thank the reviewers for their helpful comments on the presentation.

References

[1] Koester, D. A., Markus, K. W., and Walters, M. D., "MEMS: Small Machines for the Microelectronics Age," *Computer*, Vol. 29, No. 1, 1996, pp. 93–94.

[2] Robinson, E. Y., Helvajian, H., and Janson, S. W., "MEMS: Macro Growth for Micro Systems," *Aerospace America*, Vol. 33, Feb. 1995, pp. 9, 10.

[3] O'Connor, L., "MEMS: Microelectromechanical Systems," *Mechanical Engineering Journal*, Vol. 114, No. 2, 1992, pp. 205–217.

[4] Lammerink, T. S. J., Elwenspoek, M., and Fluitman, J. H. J., "Integrated Micro-Liquid Dosing System," *Proceedings of the Micro Electro Mechanical Systems* (Fort Lauderdale, FL), Inst. of Electrical and Electronics Engineers, New York, 1993, pp. 254–259.

[5] Gass, V., Van der Schoot, B. H., and De Rooij, N. F., "Nanofluid Handling by Micro-Flow-Sensor Based on Drag Force Measurements," *Proceedings of the Micro Electro Mechanical Systems* (Fort Lauderdale, FL), Inst. of Electrical and Electronics Engineers, New York, 1993, pp. 167–172.

[6] Guckel, H., Christenson, T. R., Skrobis, K. J., Jung, T. S., Klein, J., Hartojo, K. V., and Widjaja, I., "A First Functional Current Exited Planar Rotational Magnetic Micromotor," *Proceedings of the Micro Electro Mechanical Systems* (Fort Lauderdale, FL), Inst. of Electrical and Electronics Engineers, New York, 1993, pp. 7–11.

[7] Tonucci, R. J., Justus, B. L., Campillo, A. J., and Ford, C. E., "Nanochannel Array Glass," *Science*, Vol. 258, Oct. 1992, pp. 783–785.

[8] Pearson, D. H., and Tonucci, R. J., "Nanochannel Glass Replica Membranes," *Science*, Vol. 270, Oct. 1995, pp. 68–70.

[9] Beskok, A., and Karniadakis, G. E., "Simulation of Heat and Momentum Transfer in Complex Microgeometries," *Journal of Thermophysics and Heat Transfer*, Vol. 8, No. 4, 1994, pp. 647–655.

[10] Bird, G. A., *Molecular Gas Dynamics and the Direct Simulation of Gas Flows*, Oxford Univ. Press, Oxford, England, 1994.

[11] Bird, G. A., "Direct Simulation of Gas Flows at the Molecular Level," *Communications in Applied Numerical Methods*, Vol. 4, No. 2, 1988, pp. 165–172.

[12] Moss, J. N., Mitcheltree, R. A., Wilmoth, R. G., and Dogra, V. K., "Hypersonic Blunt Body Wake Computations Using DSMC and Navier-Stokes Solvers," AIAA Paper 93-2807, July 1993.

[13] Wilmoth, R. G., Mitcheltree, R. A., Moss, J. N., and Dogra, V. K., "Zonally-Decoupled DSMC Solutions of Hypersonic Blunt Body Wake Flows," AIAA Paper 93-2808, July 1993.

[14] Dogra, V. K., Moss, J. N., Wilmoth, R. G., Taylor, J. C., and Hassan, H. A., "Effects of Chemistry on Blunt Body Wake Structure," AIAA Paper 94-0352, Jan. 1994.

[15] Carlson, A. B., and Hassan, H. A., "Radiation Modeling with Direct Simulation Monte Carlo," *Journal of Thermophysics and Heat Transfer*, Vol. 6, No. 4, 1992, pp. 631–636.

[16] Pfahler, J., Harley, J., and Bau, H., "Gas and Liquid Flow in Small Channels," *Micromechanical Sensors, Actuators, and Systems*, DSC-Vol. 32, American Society of Mechanical Engineers, New York, 1991, pp. 49–59.

[17] Liu, J. Q., Tai, Y. C., Pong, K. C., and Ho, C. M., "Micromachined Channel/Pressure Sensor Systems for Micro Flow Studies," *7th International Conference on Solid-State Sensors and Actuators*, Inst. of Electrical and Electronics Engineers, New York, 1993, pp. 995–998.

[18] Pong, K. C., Ho, C. M., Liu, J. Q., and Tai, Y. C., "Non-Linear Pressure Distribution in Uniform Microchannels," *Application of Microfabrication to Fluid Mechanics*, FED-Vol. 197, American Society of Mechanical Engineers, New York, 1996, pp. 51–56.

[19] Piekos, E. S., and Breuer, K. S., "DSMC Modeling of Microchannel Devices," AIAA Paper 95-2089, June 1995.

[20] Oh, C. K., Oran, E. S., and Cybyk, B. Z., "Microchannel Flows Computed with the DSMC-MLG," AIAA Paper 95-2090, June 1995.

[21] Ahn, J. C., "Heat Transfer and Flow Fields in Microchannels Using the DSMC Simulation Method," Ph.D. Dissertation, George Washington Univ., Washington, DC, 1996.

[22] Cheng, H. K., "Viscous Hypersonic Blunt-Body Problems and the Newtonian Theory," *Hypersonic Flow*, edited by J. G. Hall, Cornell Univ. Press, Ithaca, New York, 1966.

[23] Shapiro, A. H., *The Dynamics and Thermodynamics of Compressible Fluid Flow*, Vols. 1 and 2, Ronald, New York, 1954.

[24] John, J. E. A., *Gas Dynamics*, Allyn and Bacon, Boston, 1984.

[25] Bird, G. A., *The G2/A3 Program System Users Manual*, Version 1.8, G. A. B. Consulting Pty Ltd., Killona, Australia, 1992.

[26] Arkilic, E., and Breuer, K. S., "Gaseous Flow in Small Channels," AIAA Paper 93-3270, July 1993.

[27] Beskok, A., Trimmer, W., and Karniadakis, G. E., "Rarefaction and Compressibility Effects in Microflows: Simulations and Proposed Benchmark Experiments," Brown Univ. Rept., Providence, RI, March 1995.

[28] Beskok, A., Trimmer, W., and Karniadakis, G. E., "Rarefaction, Compressibility and Thermal Creep Effects in Microflows," *Proceedings of the ASME Dynamics Systems and Control Division*, DSC-Vol. 57-2, 1995, pp. 887–892.